JOURNAL OF AIRCRAFT
Vol. 40, No. 6, November–December 2003

Wave-Drag Characteristics of an Over-the-Wing Nacelle Business-Jet Configuration

Michimasa Fujino* and Yuichi Kawamura†
Honda R&D Americas, Inc., Greensboro, North Carolina 27409

This paper presents the wave-drag characteristics of an over-the-wing nacelle configuration. The flow over the wing is accelerated such that the aerodynamic interference between the nacelle and the wing is critical in the transonic flight regime. In general, locating nacelles over the wing causes an unfavorable aerodynamic interference and induces a strong shock wave, which results in a lower drag-divergence Mach number. If the nacelle is located at the optimum position relative to the wing, however, the shock wave can be minimized, and drag divergence occurs at a Mach number higher than that for the clean-wing configuration. Theoretical analyses and experimental measurements demonstrate that a wave-drag reduction can be achieved by locating the nacelle front face near the shock-wave position on the wing.

Nomenclature

b	=	wing span, m (ft)
C_D	=	airplane drag coefficient
$(C_D)_{M=0.7}$	=	airplane drag coefficient at $M = 0.7$
C_{DW}	=	airplane wave-drag coefficient
C_L	=	airplane lift coefficient
C_M	=	airplane pitching-moment coefficient
C_p	=	pressure coefficient
c	=	chord, m (ft)
D	=	airplane drag, kgf (lbf)
h	=	maximum height of nacelle, m (ft)
L	=	airplane lift, kgf (lbf)
M	=	freestream Mach number
M_{DD}	=	drag-divergence Mach number, Mach number where $d(C_D)/dM = 0.1$
w	=	maximum width of nacelle, m (ft)
X	=	chordwise distance from wing leading edge to nacelle front face, m (ft)
x	=	chordwise distance from wing leading edge, m (ft)
Y	=	spanwise distance from fuselage surface to nacelle inboard surface, m (ft)
y	=	spanwise distance from fuselage centerline, m (ft)
Z	=	vertical distance from wing upper surface to nacelle lower surface, m (ft)
η	=	nondimensional span station, $y/(b/2)$

Introduction

THE small jet is becoming very popular among business people. Market surveys show that demand for comfort, in particular a large cabin, is critical to the success of business-jet development. Mounting the engines on the wing instead of the fuselage is one way to maximize the cabin size by removing the engine support structure from the fuselage. If the engines are installed under the wing, however, problems such as ground clearance cannot be avoided for a small business-jet configuration. On the other hand, if the nacelles are installed over the wing, the drag caused by aerodynamic interference increases, especially at high speeds. If the aerodynamic interference can be minimized and the drag-divergence characteristics improved for such a configuration, both a large cabin and high cruise efficiency are possible.

Much research has been conducted to improve drag-rise characteristics by minimizing interference and optimizing the integration of the engine nacelle and the aircraft. Several investigations of the aerodynamic interference between the nacelles and the wing upper surface have been conducted.[1–3] In Ref. 1 it was shown that the drag increment caused by the addition of a nacelle and pylon could be reduced to the level of only the additional skin-friction drag; thus, the premature drag break that was a consequence of the adverse nacelle-pylon interference was eliminated by proper design. The results also showed that the drag increment for a certain configuration with nacelles and pylons was lower than a configuration without nacelles and pylons. It was concluded that this result was probably caused by some minor refinement of the outboard wing, and no further detailed investigation was conducted. In Ref. 2 it was shown that the presence of nacelles over the wing produced a beneficial interference with respect to drag and, in some cases, the drag of the wing body with nacelles was lower than the baseline wing body. In this investigation, however, the nacelles were not metric, and, therefore, it was difficult to separate the effects conclusively.

Another example of a configuration study to improve drag-rise characteristics is the shock body of Ref. 4. This investigation showed that the addition of special bodies on the upper surface of a wing improved the drag-rise characteristics.

All of these investigations indicate that there is a possibility that the drag-rise characteristics can be improved by taking advantage of a favorable interference between two components and that the drag-divergence Mach number can be increased.

The present paper describes an over-the-wing nacelle configuration that improves the drag-rise characteristics and increases the drag-divergence Mach number through favorable aerodynamic interference between the natural-laminar-flow wing and the nacelle. The nacelle is used as an additional body to give a favorable interference effect. Systematic analyses and experiments were conducted to determine the optimum location of the nacelle relative to the wing and the fuselage. The results show that the optimum over-the-wing nacelle configuration can result in drag-rise characteristics that are better than those of the clean configuration without nacelles and pylons.

There have been few examples of the over-the-wing engine configuration to date,[5,6] and these airplanes were designed for subsonic flight. The present investigation is focused on mid- to high-speed flight.

Presented as Paper 2003-0933 at the AIAA 41st Aerospace Sciences Meeting and Exhibit, Reno, NV, 6 January 2003; received 3 April 2003; revision received 30 July 2003; accepted for publication 30 July 2003.

*Chief Engineer, 6423B Bryan Boulevard; mfujino@oh.hra.com; fujinox@alles.or.jp. Member AIAA.

†Research Engineer, 6423B Bryan Boulevard; ykawamura@oh.hra.com. Member AIAA.

Theoretical Results

Method

A three-dimensional Euler solver[7,8] was used to evaluate the interference between the wing and the nacelle. The code solves the three-dimensional Euler equations combined with the state equation. Symmetrical schemes are used in the spatial discretization, and the dissipative terms are added to increase numerical stability. The discretized equations are solved by a modified, four-stage, Runge–Kutta, time-marching scheme with residual smoothing. The code uses a multigrid-calculation procedure with an equally spaced, Cartesian mesh structure, including local refinement.[9] Because it uses local computational grids and these grids need not be aligned with the surface, the modeling of the geometry is greatly simplified, which allows the geometry to be changed quickly and efficiently. The wave drag is obtained from the integration of the entropy production on a plane just downstream of the shocks.[10]

Design Studies

Design studies were conducted for the wing-body-nacelle configuration of a small business jet to evaluate the aerodynamic interference between the nacelle and the wing. The basic configuration is shown in Fig. 1. The wing has a quarter-chord sweep of 17 deg and a taper ratio of 0.348. The airfoil has a thickness of approximately 10% chord and exhibits a favorable pressure gradient up to 45% chord on the upper surface at a Mach number of 0.73. The use of a natural-laminar-flow airfoil reduces the drag-divergence Mach number relative to that for a turbulent-flow airfoil, but the profile drag is greatly reduced. The same airfoil is used from root to tip. The wing has 5.5 deg of washout to ensure adequate aileron effectiveness at high angles of attack. A minimal root fairing prevents a strong shock from forming at the root before the shock forms on the remainder of the wing. Thus, the drag-divergence Mach number is not determined by the wing-root region.

The surface paneling used in the analyses is shown in Fig. 2. The analyses concentrated on the aerodynamic interference between the nacelle and the wing, and, therefore, the horizontal tail was not modeled. A total of 802,547 grid points were used for the over-the-wing nacelle configuration. A flow-through nacelle was used to compare the computational results to the wind-tunnel data. Powered-nacelle conditions were also analyzed by simulating the inlet velocity for a representative configuration to evaluate the effect of the inlet condition on the wave drag. The three major geometric variables in this study, illustrated in Fig. 3, are 1) the chordwise distance X from the leading edge of the wing to the front face of the nacelle, 2) the vertical distance Z from the wing upper surface to the nacelle lower surface, and 3) the spanwise distance Y from the fuselage surface to the nacelle inboard surface. All of the computations were performed for an airplane lift coefficient of 0.4, which corresponds to a typical cruise condition of the airplane under study. The lift coefficient for various configurations was maintained by adjusting the angle of attack.

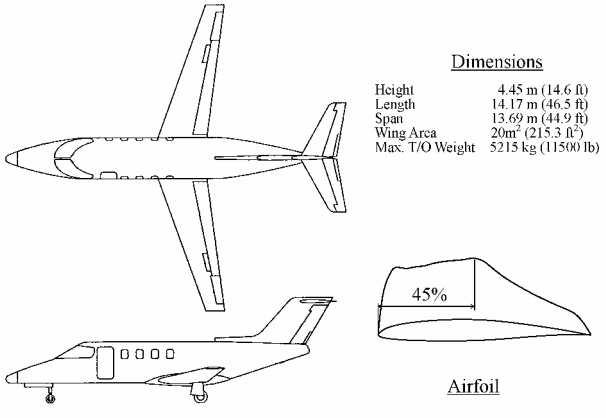

Fig. 1 Basic configuration without engines.

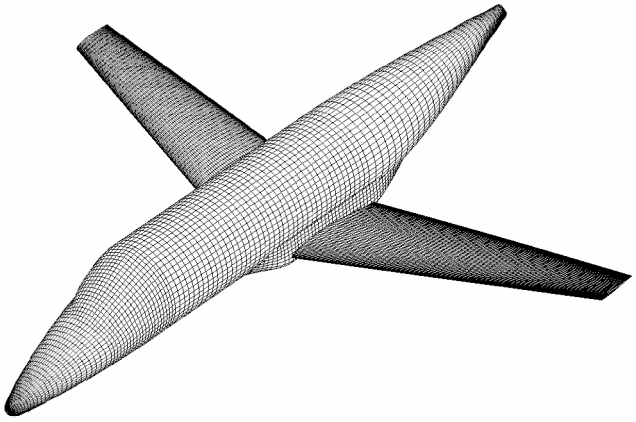

a) Clean configuration (13,004 panels)

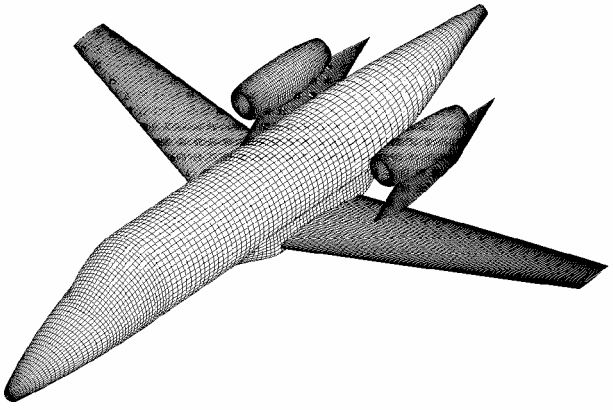

b) Over-the-wing nacelle configuration (21,472 panels)

Fig. 2 Surface paneling.

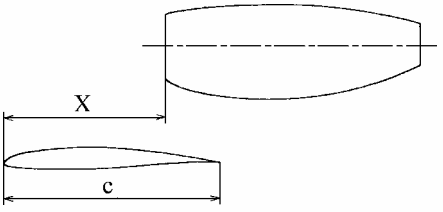

a) Chordwise distance

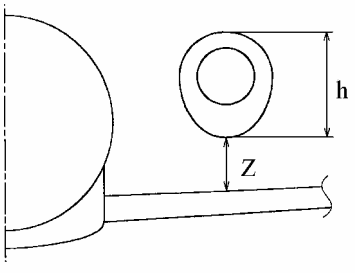

b) Vertical distance

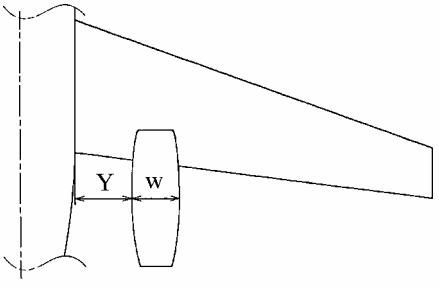

c) Spanwise distance

Fig. 3 Three parameters in study.

Effect of Nacelle Location on Wave Drag

The effects of the chordwise and vertical nacelle locations on the wave drag at a Mach number of 0.78 are shown in Fig. 4 at a spanwise location Y/w of 0.72. This analysis was performed without pylons. The wave drag is minimized when the nacelle front face is located at about $X/c = 0.8$. The wave-drag reduction is greatest when the nondimensional vertical distance Z/h between the nacelle and the wing is less than one. The effects of the chordwise and spanwise locations of the nacelle on the wave drag are shown in Fig. 5 at a vertical location Z/h of 0.5. Again the wave drag is minimized when the nacelle front face is located at about $X/c = 0.8$. The effect of chordwise location on the wave drag at different Mach numbers is shown in Fig. 6. The drag reduction as a result of the optimal chordwise location of the nacelle increases with increasing Mach number. The effect of chordwise nacelle location on the wing pressure distribution is shown in Fig. 7. At a span station η of 0.18, a shock wave occurs at about 70% chord on the clean wing. If the front face of the nacelle is located near the shock position for the clean wing (i.e., $X/c = 0.75$, 0.8), the shock becomes weaker. This results in a higher drag-divergence Mach number than that of the clean-wing configuration (Fig. 8). If the nacelle front face is located at the midchord of the wing, a strong shock forms toward the trailing edge of the wing, which results in higher wave drag and a lower drag-divergence Mach number, as shown in Fig. 8. These results demonstrate that the strength and the location of the shock as well as the wave drag can be favorably influenced by the placement of the nacelle relative to the wing.

The effect of the vertical distance from the wing to the nacelle on the wing pressure distribution is shown in Fig. 9. If the nacelle is placed very close to the wing upper surface ($Z/h = 0.1$), a strong shock forms between the wing and the nacelle near the trailing edge of the wing. This causes high wave drag and boundary-layer separation. On the other hand, if the nacelle is placed far above the wing upper surface ($Z/h = 1.5$) the wing pressure distribution is not significantly influenced by the flowfield around the nacelle, and the wave-drag reduction caused by the nacelle disappears.

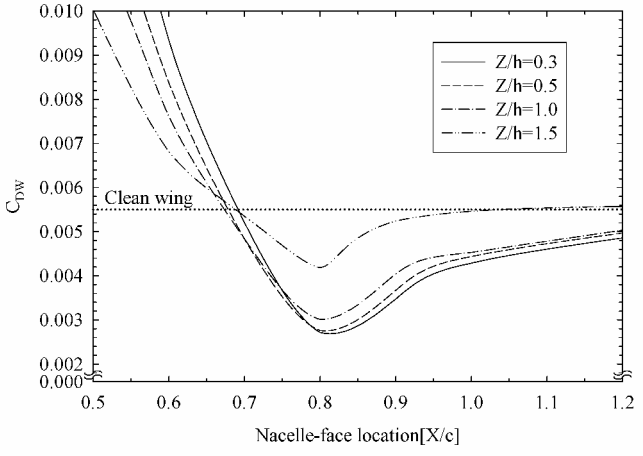

Fig. 4 Effects of vertical and chordwise locations of nacelle on wave drag for $M = 0.78$ and $Y/w = 0.72$.

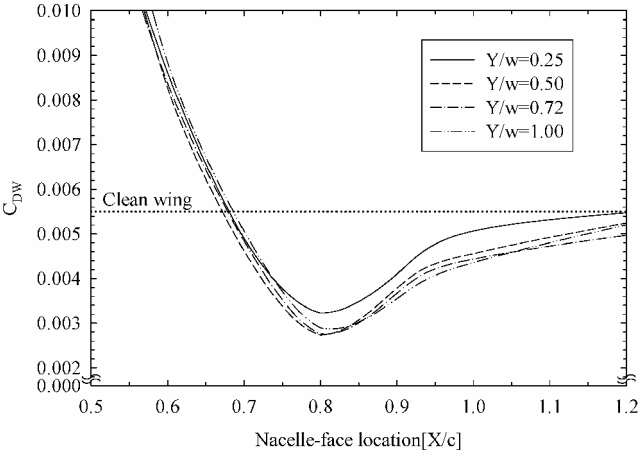

Fig. 5 Effects of spanwise and chordwise locations of nacelle on wave drag for $M = 0.78$ and $Z/h = 0.5$.

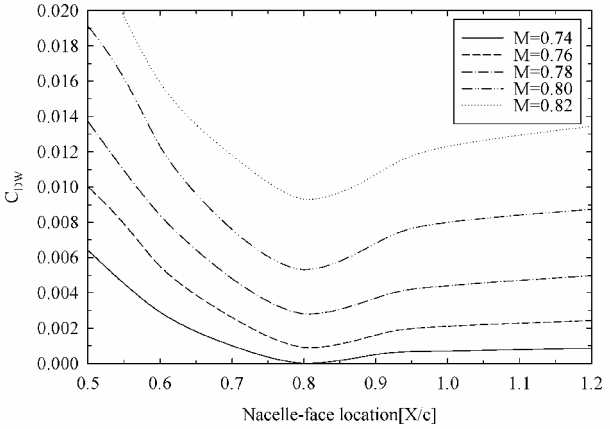

Fig. 6 Effect of Mach number on wave drag for $Z/h = 0.5$ and $Y/w = 0.72$.

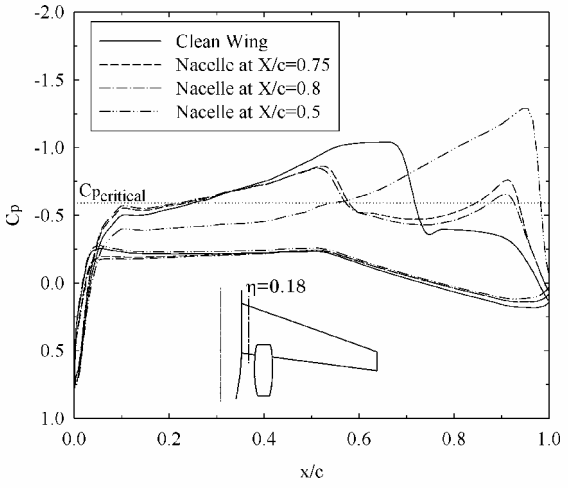

a) $\eta = 0.18$

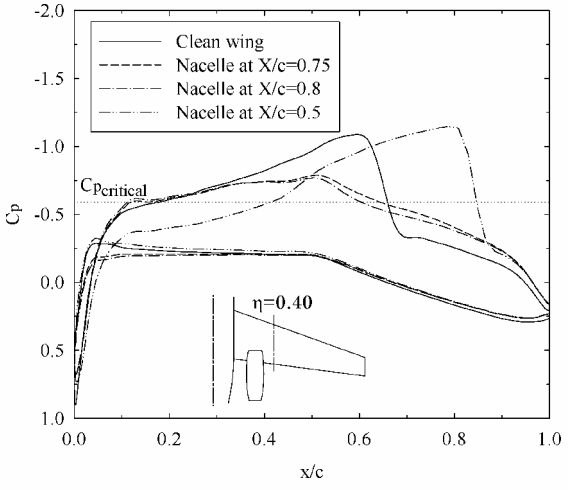

b) $\eta = 0.40$

Fig. 7 Effect of chordwise nacelle location on pressure distribution for $M = 0.75$, $Z/h = 0.5$, and $Y/w = 0.72$.

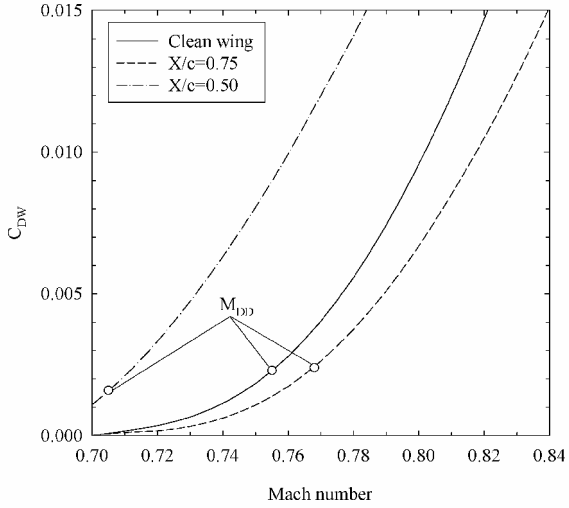

Fig. 8 Wave drag of over-the-wing nacelle configuration for $Z/h = 0.5$ and $Y/w = 0.72$.

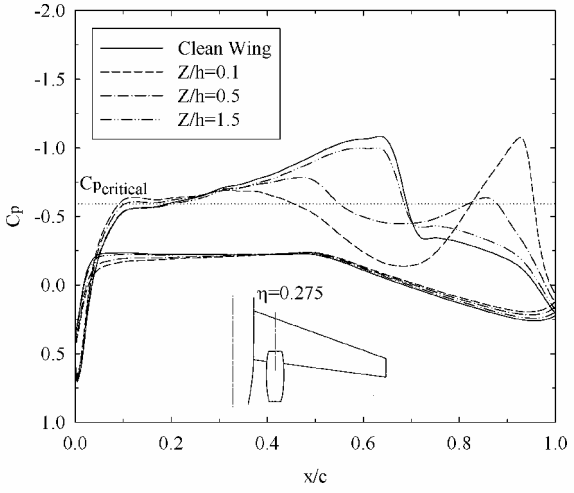

Fig. 9 Effect of vertical distance from wing to nacelle on pressure distribution on wing for $M = 0.75$, $X/c = 0.75$, $Y/w = 0.72$, and $\eta = 0.275$.

Effect of Power

To evaluate the effect of a powered nacelle on the wave drag, the inlet condition was simulated by assuming that the inlet Mach number is maintained at 0.45 at the cruise condition. The exit condition was simulated by assuming the exit Mach number is equal to 1.0. The effect of power on the wing pressure distribution is shown in Fig. 10. The engine inlet boundary condition gives a slightly greater blockage effect and a slightly greater effect of the nacelle on the wing pressure distribution. The effect of power on the wave drag, however, is small, as shown in Fig. 11.

Effect of Pylon

A pylon was then added to the over-the-wing nacelle configuration, as shown in Fig. 12. The NACA 65-008 airfoil was selected for the shape of the pylon. The effect of the pylon on the wing pressure distribution is shown in Fig. 13. The shock strength on the wing is weaker with the pylon. The effect of the pylon on the wave drag is shown in Fig. 14. The wave drag with the pylon becomes lower than that without the pylon because the pylon reduces the velocity upstream. This result shows that adding the pylon produces a favorable aerodynamic effect at the optimal over-the-wing nacelle location.

Experimental Results

Test Apparatus

Transonic wind-tunnel tests were conducted in the Boeing Transonic Wind Tunnel (BTWT) using a $\frac{1}{8}$-scale model (Fig. 15). The

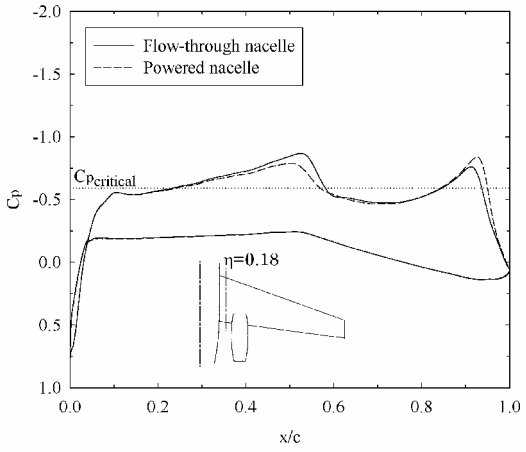

a) $\eta = 0.18$

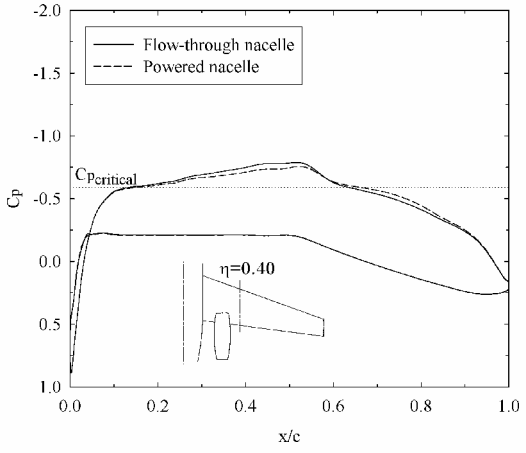

b) $\eta = 0.40$

Fig. 10 Effect of power on wing for $M = 0.75$, $Z/h = 0.5$, $Y/w = 0.72$, and $X/c = 0.75$.

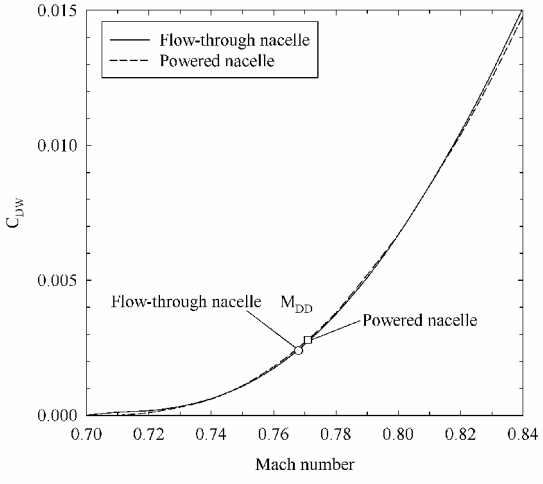

Fig. 11 Effect of power on wave drag for $Z/h = 0.5$, $Y/w = 0.72$, and $X/c = 0.75$.

three view of the model, the wing geometry, and the orifice locations are shown in Fig. 16. The pressures were measured using a Hyscan Electronic Pressure Scanning System. Flight simulation chamber testing was conducted to determine the nacelle internal drag at the BTWT operating conditions. This chamber is instrumented to provide the data necessary to calculate the flow through the nacelle and the velocity coefficient. The model was mounted on a swept strut, and an internal balance was used to measure the forces and moments. The calculated nacelle internal drag was used to correct

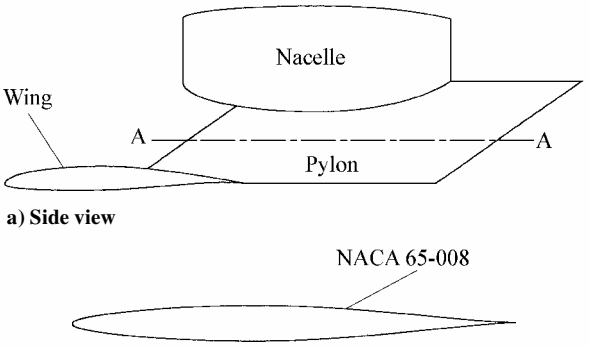

a) Side view

b) Section AA

Fig. 12 Side view and cross section of pylon.

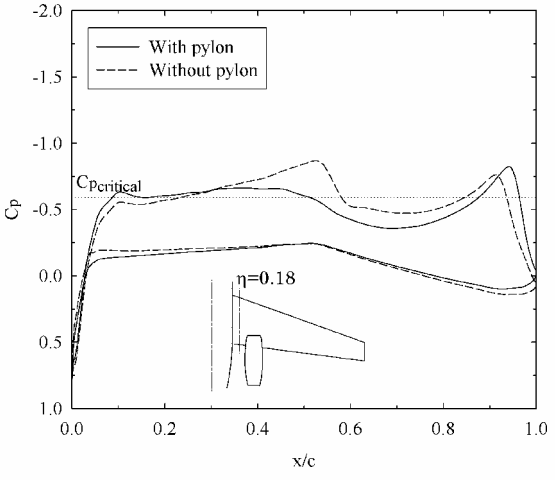

a) $\eta = 0.18$

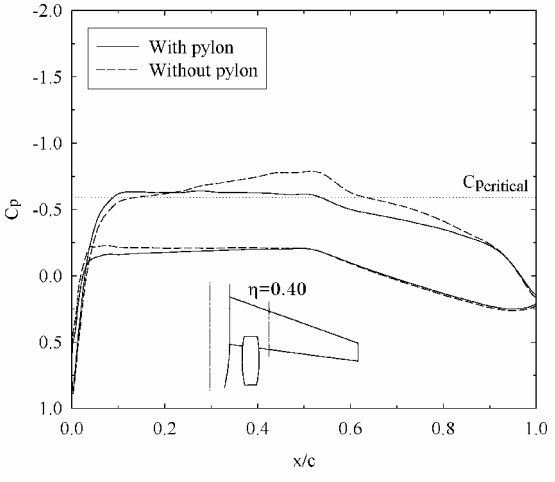

b) $\eta = 0.40$

Fig. 13 Effect of pylon on wing pressure distribution for $M = 0.75$, $Z/h = 0.5$, $Y/w = 0.72$, and $X/c = 0.75$.

the data obtained from the internal balance. A strut-cavity correction has been applied to the data. The drag measurements have been corrected for buoyancy effects. All of the test runs were made with transition disks placed at 10% chord on the wing, near the leading edge of the nacelle and the pylon and near the fuselage nose to fix transition. The Mach number was varied from 0.70 to 0.84 in increments of 0.01. All measurements were made at a lift coefficient of 0.4. The eight configurations are shown in Fig. 17 and described in Table 1. It should be noted that the nacelle front face for configurations 4 and 5 is located at $X/c = 0.75$ for the wind tunnel test due to a constraint from the full-scale aircraft structural design. As shown in the theoretical results, however, this location is very close

Table 1 Configuration definitions

Configuration	Description	Pylon	X/c	Y/w	Z/h
1	Clean wing	None	——	——	——
2	Over-the-wing nacelle/forward	Basic	−1.14	0.72	0.5
3	Over-the-wing nacelle/mid	Basic	0.5	0.72	0.5
4	Over-the-wing nacelle/aft	Basic	0.75	0.72	0.5
5	Over-the-wing nacelle/aft	Contoured (aligned with local flow)	0.75	0.72	0.5
6	Rear-fuselage mounted nacelle	Aligned with local flow	0.9	0.5	0.8
7	Under-the-wing nacelle/forward	Basic	−1.14	0.72	0.25
8	Under-the-wing nacelle/aft	Basic	0.8	0.72	0.25

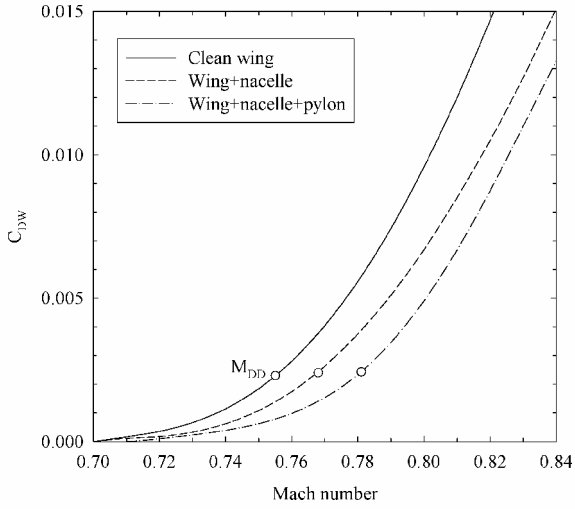

Fig. 14 Effect of pylon on wave drag for $Z/h = 0.5$, $Y/w = 0.72$, and $X/c = 0.75$.

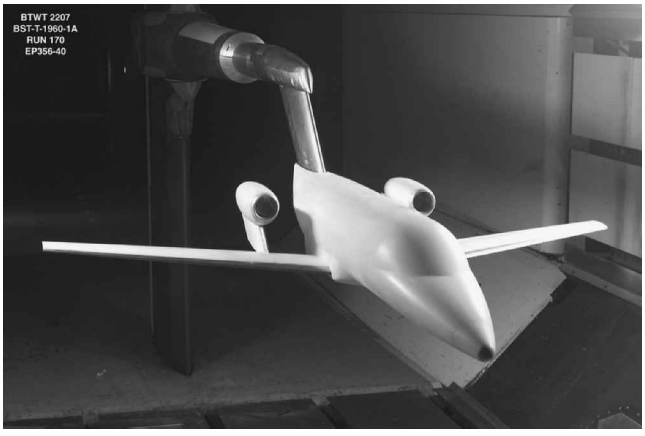

Fig. 15 Photograph of $\frac{1}{8}$-scale model installed in Boeing Transonic Wind Tunnel (BTWT).

to the optimum location and the effects of the nacelle on the pressure distribution of the wing for $X/c = 0.75$ and 0.8 are similar.

Pressure Distributions

The wing pressure distributions for configurations 1–4 are shown in Fig. 18. Comparisons of the theoretical and experimental pressure distributions for the over-the-wing nacelle/aft configuration 4 are shown in Fig. 19. The agreement is generally good. Theoretical pressure distribution with boundary layer effect is also shown in this figure. An integral boundary layer calculation along surface

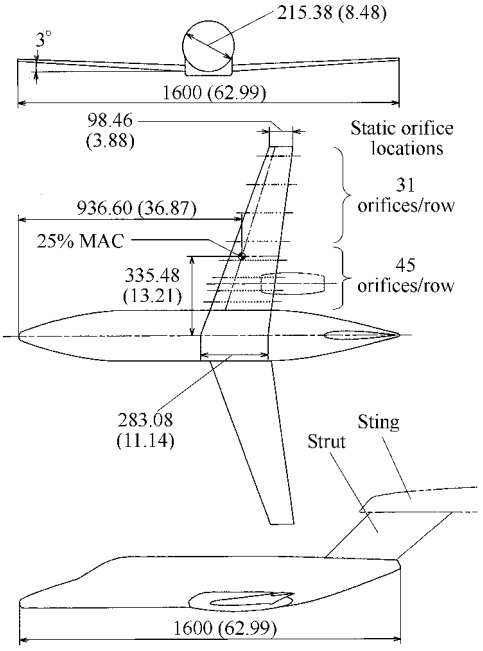

Fig. 16 Drawing of wind-tunnel model. All dimensions are in millimeters (inches).

streamlines is performed. The inviscid surface boundary condition is modified based upon the rate of growth of the boundary layer displacement thickness and is manifested via surface transpiration velocity.[7] The transition location is fixed at 10% chord of the wing. The theoretical pressure distribution with boundary layer effect is in better agreement with the experimental pressure distribution. Comparisons for the other configurations are similar.

Drag-Rise Characteristics

The drag-rise characteristics of configurations 1–4 are shown in Fig. 20. The subsonic drag coefficient ($M = 0.7$) has been subtracted from the drag coefficient for each configuration. For the nacelle front face located at the midchord of the wing (configuration 3), the drag-divergence Mach number is relatively low, whereas for the nacelle located near the shock position (configuration 4) the drag-divergence Mach number is higher than that for the clean-wing configuration 1.

The comparison of the theoretical and experimental drag-rise characteristics is shown in Fig. 21. The theory without boundary layer predicts slightly higher wave drag than that of the experiments. The drag-rise characteristic is, however, similar to that of the experiment. The wave drag obtained from theory with boundary layer effect agrees well with that of the experiment up to the drag-divergence Mach number, above which the experimental drag coefficients increase more rapidly. This result is obtained because the theoretical method does not account for the additional drag caused by the separation that occurs at higher Mach numbers.

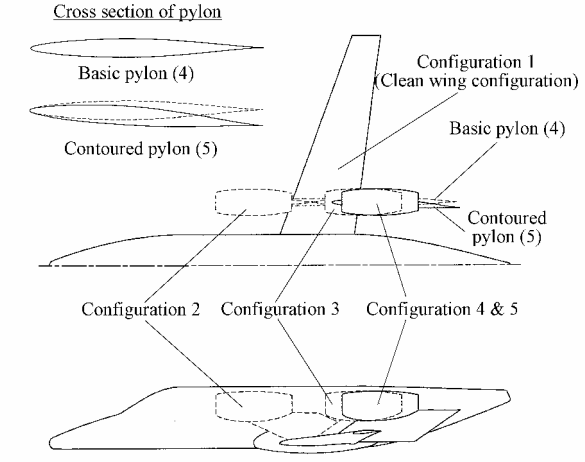

a) Clean wing and over-the-wing nacelle

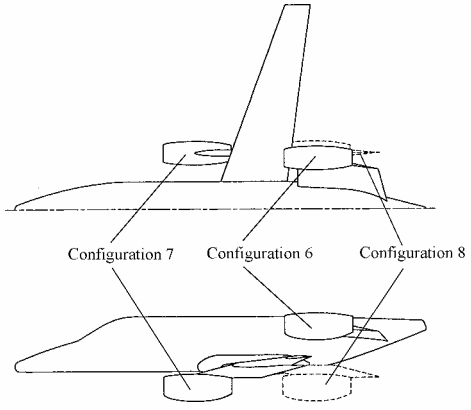

b) Fuselage-mounted nacelle and under-the-wing nacelle

Fig. 17 Model configurations.

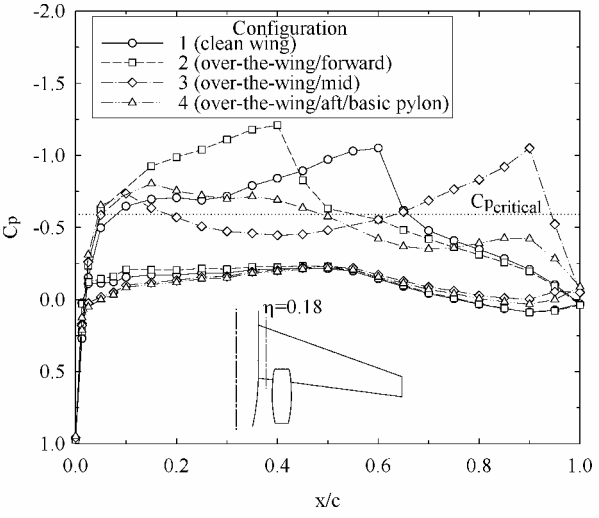

a) $\eta = 0.18$

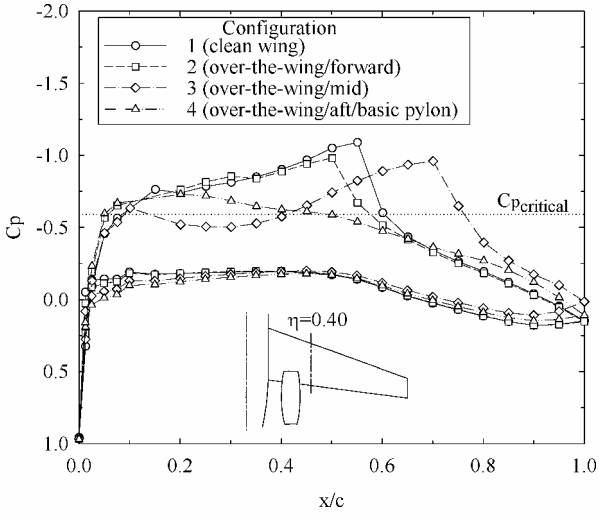

b) $\eta = 0.40$

Fig. 18 Wing pressure distributions at $M = 0.75$ and $C_L = 0.4$.

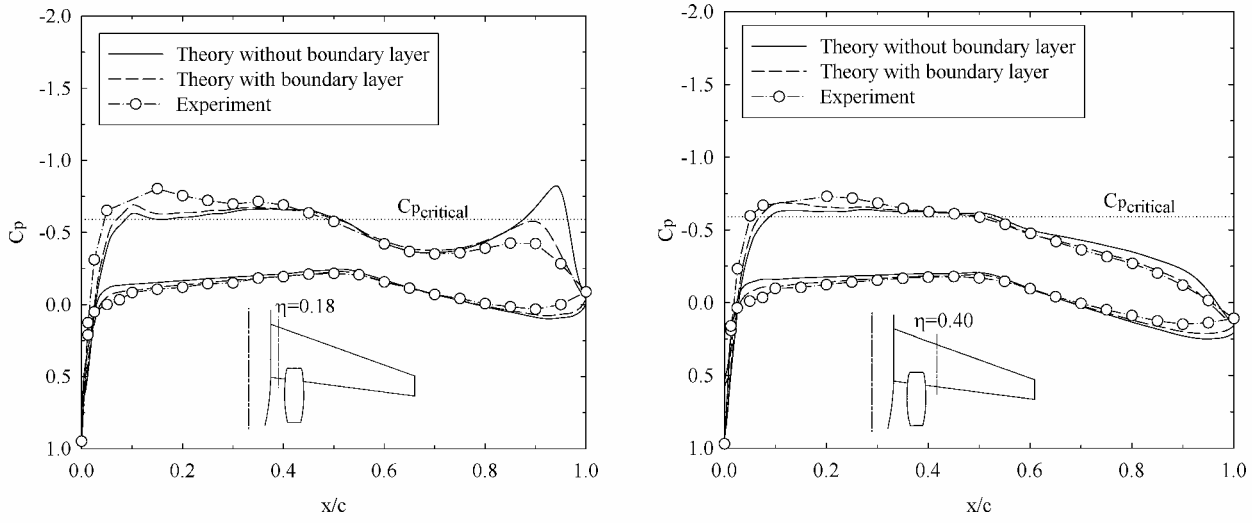

a) $\eta = 0.18$ b) $\eta = 0.40$

Fig. 19 Comparison of theoretical and experimental pressure distributions for configuration 4: $M = 0.75$, and $C_L = 0.4$.

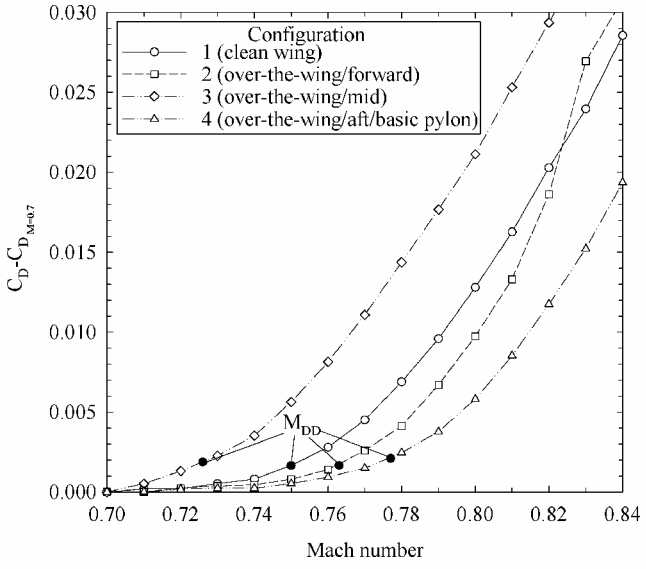

Fig. 20 Drag-rise characteristics of configurations 1–4.

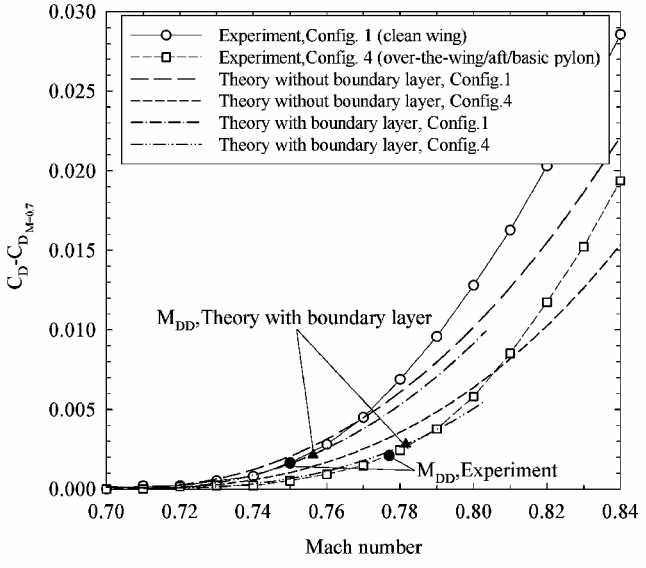

Fig. 21 Comparison of theoretical and experimental drag-rise characteristics.

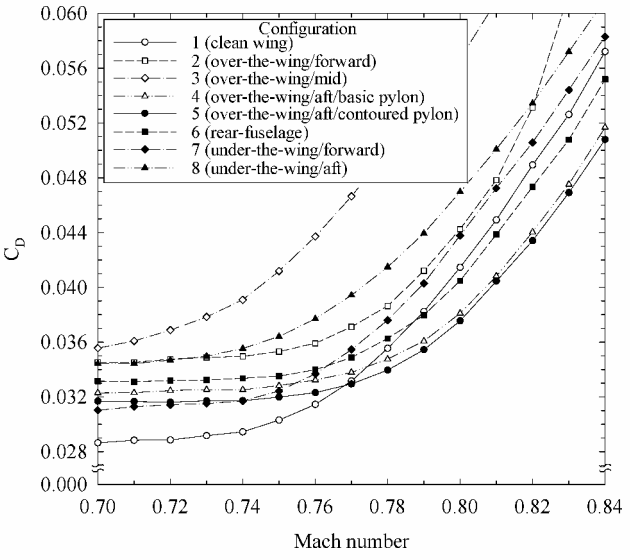

Fig. 22 Drag coefficients of all configurations.

The drag coefficients of all eight configurations are shown in Fig. 22. Configurations 4 and 5 achieve the highest drag-divergence Mach numbers, but configuration 5 exhibits lower drag at lower Mach numbers ($M = 0.7$). This result shows that the contoured pylon, which is designed to be aligned with the local flow, decreases the interference drag at low to mid-speeds.

The results also show that the drag coefficient of the conventional, rear-fuselage-mountednacelle configuration 6 is higher than that of configuration 5. To provide a valid comparison between the over-the-wing nacelle configuration and the fuselage-mounted nacelle configuration, the total wetted areas of configurations 5 and 6 are the same. The pylon thickness and the distance between the pylon and the fuselage are designed to delay the formation of a shock in the pylon-fuselage region until after the shock has formed on the remainder of the wing. In addition, the pylon for configuration 6 is aligned with the local flow to minimize interference, as was done for configuration 5.

Discussion

Favorable Interference of Over-the-Wing Nacelle Configuration

Both the theoretical and experimental results show that there is an optimum chordwise location of the nacelle relative to the wing for which favorable aerodynamic interference and a wave-drag reduction occur. These results are explained as follows. The flow forward

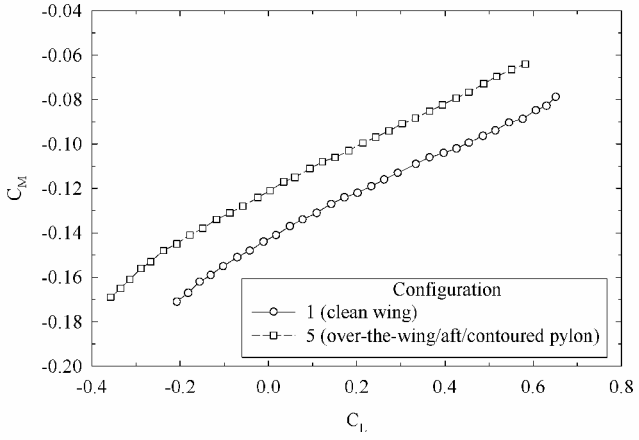

Fig. 23 Pitching-moment coefficients at $M = 0.75$.

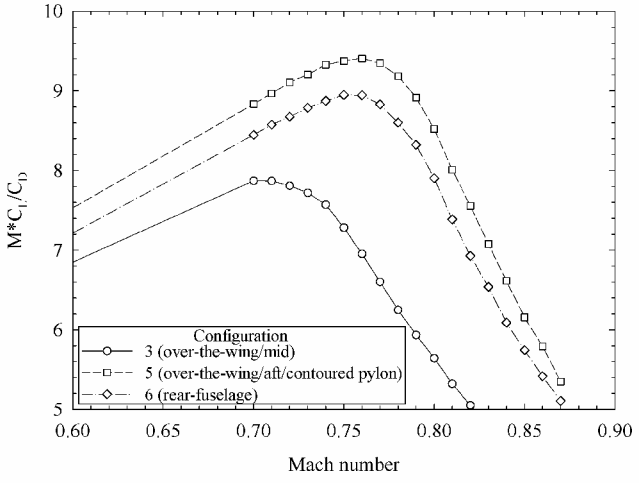

Fig. 24 Range parameter.

of the nacelle is decelerated by the nacelle. The decelerated flow is superimposed on the accelerated flow just ahead of the shock on the wing. The two superimposed flows result in a weaker shock and a higher drag-divergence Mach number (Fig. 20). Favorable aerodynamic interference occurs if the vertical distance between the wing and the nacelle is within the range $0.3 < Z/h < 0.5$ and the nacelle face is located near the shock position on the wing. If the nacelle is located too close to the wing upper surface ($Z/h < 0.1$), a strong shock forms between the nacelle and the wing, which results in higher drag. If the nacelle is located too high above the wing upper surface ($Z/h > 1.5$), the favorable effect from the superimposed flowfields does not occur.

Pitching Moment

The pitching-moment coefficient of the over-the-wing nacelle configuration 5 is compared to those of configuration 1 in Fig. 23. The pitching-moment coefficient of the over-the-wing nacelle configuration is less negative than those of the clean-wing configuration, and, therefore, less download on the horizontal tail is required to trim the airplane. Reduced download on the horizontal tail leads to lower trim drag.

Cruise Efficiency

The advantage of the over-the-wing nacelle configuration in cruise can be evaluated using the figure of merit $M \cdot (L/D)$, which is the range parameter of jet airplanes. The range parameters of configurations 3, 5, and 6, which were calculated from wind-tunnel test results, are shown in Fig. 24. The range parameter of the over-the-wing nacelle configuration with contoured pylon (configuration 5) is approximately 5% greater than that of the conventional, rear-mounted nacelle configuration 6 because of the lower interference drag at lower Mach numbers ($M < 0.7$) and the improved drag-divergence characteristics.

Conclusions

Theoretical and experimental results show that an over-the-wing nacelle configuration can reduce wave drag and increase drag-divergence Mach number. The nacelle front face should be located near the shock position on the clean wing, and the vertical distance between the wing and the nacelle should be about $\frac{1}{3}$ to $\frac{1}{2}$ the maximum height of the nacelle. For this nacelle location adding a pylon improves the drag-divergence characteristics, and a contoured pylon, aligned with the local flow, improves the aerodynamic interference at lower Mach numbers ($M = < 0.7$). This over-the-wing nacelle configuration reduces the cruise drag at transonic speeds without altering the original geometry of the natural-laminar-flow wing. In addition, the carry-through structure required to mount the engines on the rear fuselage is eliminated, which allows the cabin volume to be maximized.

References

[1]Bartlett, D. W., "Application of a Supercritical Wing to an Executive-Type Jet Transport Model," NASA TM-X-3251, June 1975.

[2]Reubush, D. E., "Effect of Over-the-Wing Nacelles on Wing-Body Aerodynamics," *Journal of Aircraft*, Vol. 16, No. 6, 1979, pp. 359–365.

[3]Henderson, W. P., and Abeyounis, W. K., "Aerodynamic Characteristics of a High-Wing Transport Configuration with an Over-the-Wing Nacelle-Pylon Arrangement," NASA TP-2497, July 1985.

[4]Whitcomb, R. T., "Special Bodies Added on a Wing to Reduce Shock-Induced Boundary-Layer Separation at High Subsonic Speeds," NACA TN-4293, June 1958.

[5]Kathen, H., "VFW 614, Quiet Short Haul Airliner," *AIAA 6th Aircraft Design, Flight Test, and Operations Meeting*, AIAA Paper 74-937, Aug. 1974.

[6]Fujino, M., "Aerodynamic and Aeroelastic Design of Experimental Aircraft MH02," *Proceedings of the 1994 AIAA/FAA Joint Symposium on General Aviation Systems*, Starkville, MS, May 1994, pp. 435–459.

[7]Strash, D. J., and Tidd, D. M., *MGAERO User's Manual*, Analytical Methods, Inc., Redmond, WA.

[8]Tidd, D. M., and Strash, D. J., "Application of an Efficient 3-D Multi-Grid Euler Method to Complete Aircraft Configurations," *9th AIAA Applied Aerodynamics Conference*, AIAA Paper 91-3236, Baltimore, MD, Sep. 1991.

[9]Epstein, B., Luntx, A. L., and Nachshon, A., "Multigrid Euler Solver About Arbitrary Aircraft Configurations with Cartesian Grids and Local Refinement," *9th AIAA Comoutional Fluid Dynamics Conference*, AIAA Paper 89-1960, Buffalo, NY, June 1989.

[10]Nikfetrat, K., van Dam, C. P., Vijgen, P. M. H. W., and Chang, I. C., "Prediction of Drag at Subsonic and Transonic Speeds Ising Euler Methods," *30th Aerospace Sciences Meeting and Exhibit*, AIAA Paper 92-0169, Reno, NV, Jan. 1992.